An ab initio and DFT Study of the Autoxidation of THF and THP

RSCPublishing

ARTICLE

An *ab initio* and DFT Study of the Autoxidation of THF and THP

Hiroshi Matsubara,* Syouhei Suzuki and Shun Hirano

www.rsc.org/

Tetrahydropyran (THP) is known to undergo autoxidation much more slowly than tetrahydrofuran (THF). To investigate the difference in reactivity in the autoxidation of these two ethers, *ab initio* and DFT calculations were carried out. At the BHandHLYP/aug-cc-pVDZ//BHandHLYP/cc-pVDZ level of theory, the energy barrier for hydrogen abstraction from THP is predicted to be 104.1 kJ·mol^{-1}, whereas that for THF is calculated as 94.1 kJ·mol^{-1}. Including solvation effects in the calculations lowers these barriers to 98.0 (THP) and 84.4 kJ·mol^{-1} (THF); the energy barrier for the process involving THP is smaller by 14 kJ·mol^{-1} than that for THF. While scanning the potential energy surface for the radical coupling process between the THP (or THF) radical with molecular oxygen, an energy barrier of 11.2 kJ·mol^{-1} (BHandHLYP/6-311G**) was found for the process involving the THP radical, although no barrier was found for the reaction involving THF. Analysis of the Kohn-Sham singly occupied molecular orbitals (SOMOs) in the hydroperoxy complexes reveals that the SOMO of the THP complex would be blocked by the neighbouring hydrogen atoms in the THP ring. These factors would work together to delay the autoxidation of THP.

Introduction

Ethers such as diethyl ether and tetrahydrofuran (THF) are common organic solvents that are widely used in organic synthesis. For example, the use of diethyl ether or THF is essential in some organometallic processes such as preparing Grignard reagents.[1] It is well known that ethers should be handled with care since the α-positions to the oxygen in the ethers are autoxidized easily to give explosive peroxides.[2,3] However, the rates of autoxidation are compound-dependent, and tetrahydropyran (THP) is strongly resistant towards autoxidation. Indeed, Howard and Ingold reported that THP is oxidized six times more slowly than THF, as shown in Scheme 1.[4] In addition, THP produced almost no peroxide after 30 days exposure to air, whereas THF formed 500 ppm peroxide under the same conditions.[5]

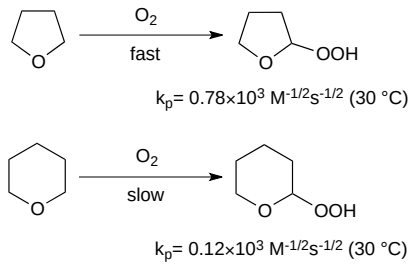

Scheme 1 Rate constants for oxidation of THF and THP.

As a result, THP can be safely used as a solvent in radical chain reactions.[5] Ryu and co-workers reported that the radical reduction and cyclization of organic bromides using Bu_3SnH in THP proceeded smoothly to afford the desired compounds in good yield. They also performed tris(trimethylsilyl)silane- and hexanethiol-mediated radical addition reactions in THP successfully (Scheme 2).

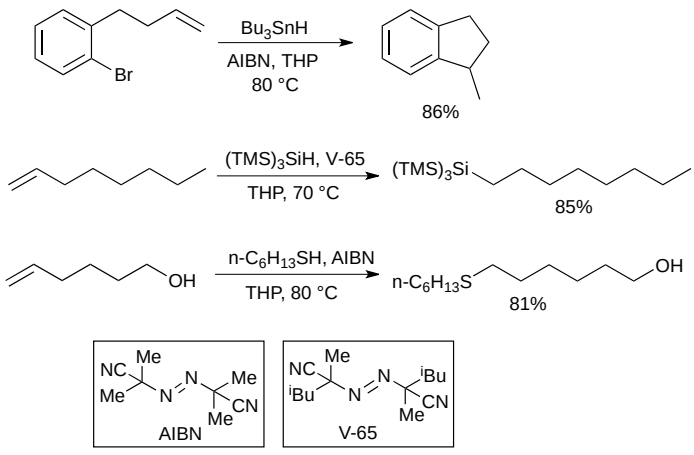

Scheme 2 Radical reactions using THP as the solvent.

THF is a five-membered ring ether, while THP is an ether containing a six-membered ring. Both appear to have almost no ring strain, and therefore, large differences in their reactivities toward radical reactions would not be expected. We have been interested[6] in the intriguing difference in reactivity between THF and THP for radical reactions, especially in the rates of autoxidation, and sought recourse to *ab initio* and DFT calculations to shed further light on the chemistry of the autoxidation processes of ethers.

The autoxidation of THF proceeds *via* a radical chain mechanism as illustrated in Scheme 3.[4] The α-hydrogen to oxygen in THF (**1a**) is abstracted by the radical initiator to give the tetrahydrofuran-2-yl radical (**2a**). Peroxy radical **3a**,[7] generated from radical **2a** and O_2, abstracts the α-hydrogen from another THF molecule to produce hydroperoxide **4a** and generate another radical **2a**. The key step in the autoxidation process is the abstraction of the α-hydrogen of THF by radical **3a**,[8,9] which is expected to be rate-determining.[4] Accordingly, we began to explore this step for both THF and THP using computational techniques.

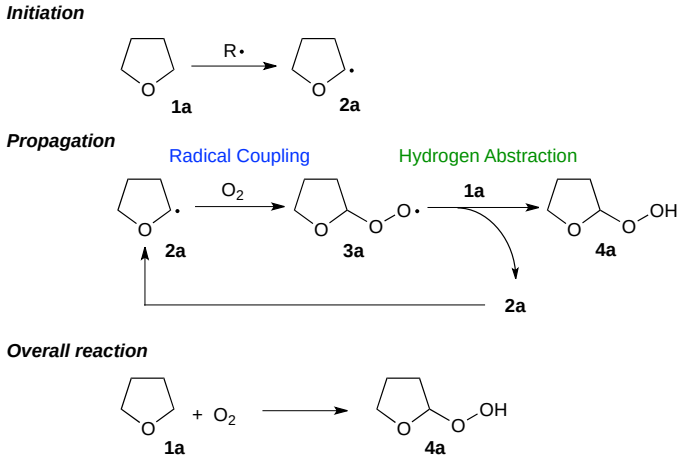

Scheme 3 Reaction mechanism of autoxidation of THF.

Methods

Ab initio and DFT calculations were carried out using the Gaussian 03 and 09 programmes.[10] Geometry optimizations were performed using standard gradient techniques at the HF, MP2, BHandHLYP, B3LYP, MPW1K,[11] MPWKCIS1K,[12] and M05[13] levels of theory using restricted (RHF, RMP2, RBHandHLYP, RB3LYP, RMPW1K, RMPWKCIS1K, RM05) and unrestricted (UHF, UMP2, UBHandHLYP, UB3LYP, UMPW1K, UMPWKCIS1K, UM05) methods for closed- and open-shell systems respectively. In every case, standard basis sets were used. All ground and transition states were verified by vibrational frequency analysis. Further single-point QCISD, CCSD(T) and calculations were performed on the MP2/6-311G** or MP2/cc-pVDZ optimized structures. The G3(MP2)-RAD[14] calculations were carried out using the MP2/cc-pVDZ and the B3LYP/6-31G* optimized geometries. Scaling factors were not applied to the G3(MP2)-RAD calculations. When correlated methods were used, calculations were carried out using the frozen core approximation. Values of $\langle s^2 \rangle$ never exceeded 0.79 before annihilation of quartet contamination. Where appropriate, zero-point vibrational energy (ZPE) corrections without scaling have been applied. Calculation including solvent effects was carried out on the BHandHLYP/aug-cc-pVDZ//BHandHLYP/cc-pVDZ level of theory using the PCM method[15] with THF as the solvent.

Optimized geometries and energies for transition and ground structures in this study (Gaussian Archive entries) are available as Electronic Supplementary Material (ESI).

Results and discussion

Abstraction of α-hydrogen in THF

We began this investigation by examining the abstraction of the α-hydrogen to oxygen in THF (**1a**) with the tetrahydrofuran-2-peroxy radical (**3a**). Inspection of the $C_8H_{15}O_4$ potential energy surface helped locate structure **6a** as the transition state for this process (Scheme 4). Complex **5a** (formed by the interaction of peroxy radical **3a** with THF) and complex **7a** (formed by the interaction of hydroperoxide **4a** with radical **2a**) are also found on the potential energy surface. The important geometric features of transition state **6a** are summarized in Fig. 1, while those of complexes **5a** and **7a** are available in Fig. S1–S2 of the ESI. The calculated energy barriers (ΔE_1, $\Delta E_2^{\ddagger}$, $\Delta E_3^{\ddagger}$, and ΔE_4, Scheme 4) together with the corresponding imaginary frequencies (ν) are listed in Table 1. Full computational details are available as the Supplementary Material.

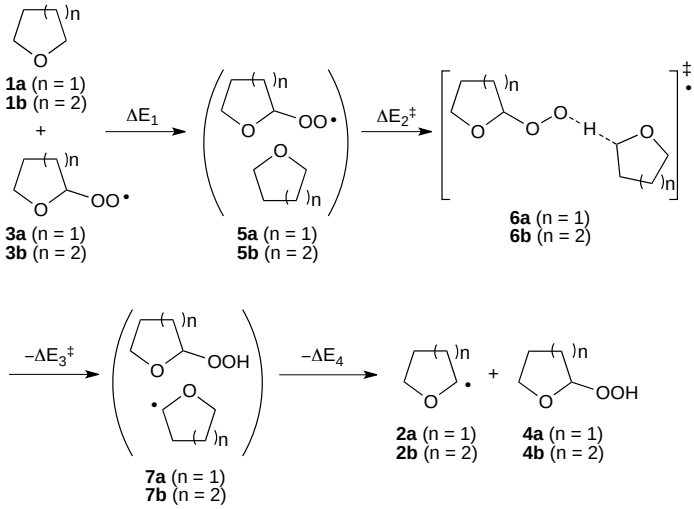

Scheme 4 Reaction pathway for the abstraction of α-hydrogen in THF and THP.

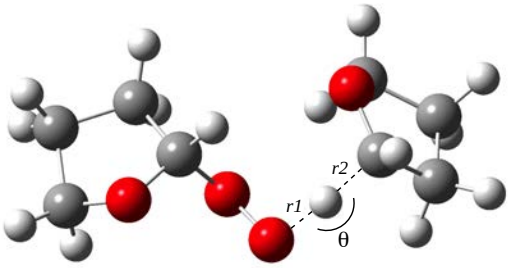

Method	*r1* (Å)	*r2* (Å)	θ (°)
HF/6-311G**	1.214	1.314	174.5
MP2/6-311G**	1.276	1.236	166.2
MP2/cc-pVDZ	1.278	1.244	164.9
BHandHLYP/6-311G**	1.222	1.296	170.9
BHandHLYP/cc-pVDZ	1.218	1.305	169.6

B3LYP/6-311G**	1.218	1.326	172.8
B3LYP/cc-pVDZ	1.210	1.340	171.1
MPW1K/cc-pVDZ	1.219	1.300	169.8
MPWKCIS1K/cc-pVDZ	1.219	1.302	170.3
M05/cc-pVDZ	1.226	1.314	168.6

Fig. 1 Optimized geometries of transition state **6a** involved in the abstraction of α-hydrogen in THF with peroxy radical **3a**.

As shown in Fig. 1, transition state **6a** is predicted to adopt a nearly collinear arrangement around the abstracted hydrogen at all levels of theory employed. The transition state (O···H) separations (*r1*) in **6a** are predicted at all levels of theory to lie in the range 1.210–1.278 Å, while the (H···C) distances (*r2*) are calculated to be 1.236–1.340 Å. Interestingly, the predicted O···H distances *via* the MP2 calculations are slightly shorter than those employing UHF and DFT methods, while the calculated H···C distances at the MP2 levels are slightly longer than those predicted with the UHF and DFT methods.

Table 1 Energy barriers (in kJ·mol^{-1}) and imaginary (ν) frequencies for abstraction of α-hydrogen in THF

Method	ΔE_1	ΔE_1 +ZPE	$\Delta E_2^{\ddagger}$	$\Delta E_2^{\ddagger}$ +ZPE	$\Delta E_3^{\ddagger}$	$\Delta E_3^{\ddagger}$ +ZPE	ΔE_4	ΔE_4 +ZPE	ν (cm^{-1})
HF/6-311G**	-13.4	-11.4	163.9	150.2	101.9	91.7	-11.3	-9.4	3375i
MP2/6-311G**	-36.0	-32.1	92.9	80.2	66.5	59.3	-30.4	-27.3	2442i
MP2/cc-pVDZ	-40.7	-36.5	94.4	81.5	64.0	56.8	-34.6	-31.3	2399i
MP2/aug-cc-pVDZ//MP2/cc-pVDZ	-39.9	--	85.3	--	67.2	--	-33.4	--	--
QCISD/6-311G**//MP2/6-311G**	-30.9	--	99.4	--	49.0	--	-25.6	--	--
QCISD/cc-pVDZ//MP2/cc-pVDZ	-35.8	--	100.9	--	48.6	--	-29.9	--	--
CCSD(T)/6-311G**//MP2/6-311G**	-34.9	--	89.2	--	44.1	--	-29.2	--	--
CCSD(T)/cc-pVDZ//MP2/cc-pVDZ	-39.5	--	91.5	--	43.7	--	-33.4	--	--
BHandHLYP/6-311G**	-22.4	-19.7	100.7	87.1	48.9	40.1	-17.5	-15.3	2191i
BHandHLYP/cc-pVDZ	-26.8	-23.2	101.0	86.3	44.8	35.7	-21.4	-18.8	2159i
BHandHLYP/aug-cc-pVDZ// BHandHLYP/cc-pVDZ	-13.0	--	94.1	--	46.8	--	-9.2	--	--
B3LYP/6-311G**	-21.6	-18.5	70.6	57.1	19.9	12.0	-14.3	-12.2	1634i
B3LYP/cc-pVDZ	-26.4	-22.9	70.9	56.7	15.2	7.0	-18.7	-16.1	1580i
MPW1K/cc-pVDZ	-21.8	-19.1	86.1	72.5	32.6	24.0	-16.5	-14.4	1928i
MPWKCIS1K/cc-pVDZ	-23.1	-19.9	84.6	70.5	32.0	23.5	-17.4	-15.2	1850i
M05/cc-pVDZ	-38.7	-35.4	91.2	76.8	31.5	22.1	-31.0	-27.7	1986i
G3(MP2)-RAD//MP2/cc-pVDZ	-32.6	-28.4	85.0	72.1	47.7	40.5	-25.9	-22.6	--
G3(MP2)-RAD//B3LYP/6-31G*	-28.6	-24.8	81.7	67.2	47.2	37.9	-24.5	-21.1	--

Inspection of Table 1 reveals that complexation of peroxy radical **3a** with THF (**1a)** affords stabilization by 13.0–40.7 kJ mol^{-1} (ΔE_1). At all levels of theory examined, the reactions are predicted to be largely endothermic, in that the calculated energy barrier ($\Delta E_3^{\ddagger}$) for the reverse reaction (Scheme 4) is always larger than that ($\Delta E_2^{\ddagger}$) for the forward process. At the HF/6-311G** level of theory, the energy barriers are calculated to be 163.9 and 101.9 kJ·mol^{-1} for the forward ($\Delta E_2^{\ddagger}$) and reverse ($\Delta E_3^{\ddagger}$) reactions associated with transition state **6a**. The inclusion of electron correlation (MP2/6-311G**) serves to lower the predicted energy barrier to 92.9 and 66.5 kJ·mol^{-1} for the reactions. At the BHandHLYP/6-311G** level of theory, the energy barriers for the reactions are calculated to be 100.7 and 48.9 kJ·mol^{-1}, respectively. The inclusion of a zero-point vibrational energy correction (ZPE) serves to decrease these barriers by about 14 and 9 kJ mol^{-1}, respectively. The B3LYP functional affords lower energy barriers by more than 15 kJ·mol^{-1} compared to other DFT methods used in this study. At the CCSD(T)/cc-pVDZ/MP2/cc-pVDZ level of theory, $\Delta E_2^{\ddagger}$ and $\Delta E_3^{\ddagger}$ are predicted to be 91.5 and 43.7 kJ mol^{-1}, respectively while values of 81.7–85.0 and 47.2–47.7 kJ mol^{-1} are calculated using the G3(MP2)-RAD methods,[14] indicating that the BHandHLYP and MPW1K calculations perform as well as higher correlation techniques with larger basis sets.

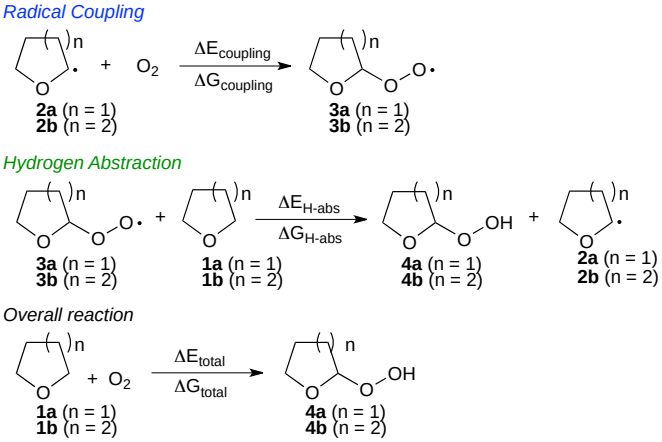

Scheme 5 Reaction energies and free energies for autoxidation of α-hydrogen in THF and THP.

The reaction energies (ΔE) and free energies (ΔG) for the radical coupling and hydrogen abstraction (Scheme 5) together with total reaction energies of the autoxidation process for THF are listed in Table 2. As shown, the coupling reaction is predicted to be exothermic while the abstraction reaction is calculated to be endothermic; the overall autoxidation reaction of THF is predicted to be exothermic. Not unexpectedly, free energies for the bimolecular reaction such as the coupling are significantly smaller (by around 40 kJ·mol^{-1}) than electronic energies together with ZPE, whereas those for the hydrogen abstraction process are very similar to the electronic energies with ZPE. Accordingly, the free energies for the overall reaction are smaller than those of the electronic energies with ZPE by some 40 kJ·mol^{-1}. Energies calculated with the BHandHLYP and B3LYP methods are in good agreement with those of higher levels of theory such as CCSD(T) and QCISD.

Table 2 Reaction energies (ΔE) and free energies (ΔG) (both in kJ·mol^{-1}) for autoxidation of THF

Method	$\Delta E_{coupling}$	$\Delta E_{coupling}$ +ZPE	$\Delta G_{coupling}$	$\Delta E_{H\text{-}abs}$	$\Delta E_{H\text{-}abs}$ +ZPE	$\Delta G_{H\text{-}abs}$	ΔE_{total}	ΔE_{total} +ZPE	ΔG_{total}
HF/6-311G**	-82.4	-64.5	-21.4	59.8	56.6	56.9	-22.6	-7.9	35.5
MP2/6-311G**	-120.1	-102.2	-59.1	20.7	16.1	20.0	-99.4	-86.1	-39.1
MP2/cc-pVDZ	-113.5	-96.0	-53.0	24.3	19.5	21.8	-89.2	-76.5	-31.2
BHandHLYP/6-311G**	-139.5	-122.1	-79.3	47.0	42.6	43.8	-92.6	-79.5	-35.5
BHandHLYP/cc-pVDZ	-139.8	-122.5	-79.8	50.8	46.1	47.0	-89.0	-76.4	-32.8
BHandHLYP/aug-cc-pVDZ// BHandHLYP/cc-pVDZ	-138.1	-121.5	-77.3	50.8	46.1	40.9	-89.0	-76.4	-36.3
B3LYP/6-311G**	-137.6	-121.4	-78.9	43.4	38.8	41.1	-94.2	-82.6	-37.8
B3LYP/cc-pVDZ	-138.8	-122.7	-80.3	47.9	43.0	44.7	-90.8	-79.7	-35.6
MPW1K/cc-pVDZ	-142.6	-125.4	-82.7	48.3	43.7	45.0	-94.3	-81.7	-37.7
MPWKCIS1K/cc-pVDZ	-139.7	-122.6	-79.8	46.9	42.3	43.5	-92.8	-80.3	-36.3
M05/cc-pVDZ	-134.5	-117.9	-75.4	52.0	47.1	48.4	-82.5	-70.8	-27.0
QCISD/cc-pVDZ//MP2/cc-pVDZ	-136.2	--	--	46.5	--	--	-89.7	--	--
CCSD(T)/cc-pVDZ//MP2/cc-pVDZ	-136.2	--	--	41.7	--	--	-94.5	--	--

Abstraction of α-hydrogen in THP

Next, we examined the abstraction of the α-hydrogen of the oxygen in THP (**1b**) by the tetrahydropyran-2-peroxy radical (**3b**) using the BHandHLYP and MPW1K levels of theory, which performed well for calculating the abstraction process for THF. Inspection of the $C_{10}H_{19}O_4$ potential energy surface located structure **6b** as the lowest energy transition state for the reaction of the α-hydrogen of THP (Scheme 4) at the BHandHLYP/6-311G**, BHandHLYP/cc-pVDZ, and MPW1K/cc-pVDZ levels of theory. Similarly to the reaction involving THF, complex **5b** formed by reaction of peroxy radical **3b** with THP, and complex **7b** formed by reaction of hydroperoxide **4b** with radical **1b**, are also found on the potential energy surface at all levels of theory employed. The important geometric features of the transition state **6b** are summarized in Fig. 2, while those of complexes **5b** and **7b** are available in Fig. S3–S4 of the ESI. Calculated energy barriers (ΔE_1, $\Delta E_2^{\ddagger}$, $\Delta E_3^{\ddagger}$ and ΔE_4, Scheme 4) together with imaginary frequencies **(ν)** are listed in Table 3. Full computational details are available as Supplementary Material.

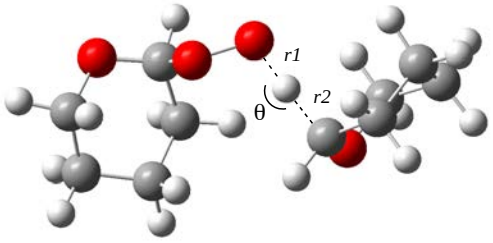

Method	*r1* (Å)	*r2* (Å)	θ (°)
BHandHLYP/6-311G**	1.211	1.313	175.7
BHandHLYP/cc-pVDZ	1.208	1.322	174.5
MPW1K/cc-pVDZ	1.204	1.324	174.3

Fig. 2 Optimized geometries of transition state **6b** involved in the abstraction of an α-hydrogen in THP with peroxy radical **3b**.

As shown in Fig. 2, transition state **6b** is also predicted to adopt a nearly collinear arrangement around the abstracted hydrogen at all levels of theory employed. The geometries of both THP rings in transition state **6b** are optimized in the chair form. The peroxy radical occupies the axial position of **3b** and abstracts a hydrogen atom from an axial position of THP. The transition state (O···H) separation (*r1*) in **6b** is predicted to be slightly shorter than that in **6a**, although the (H···C) distance (*r2*) in **6b** is calculated to be somewhat longer. These results indicate that the transition state **6b** involved in hydrogen abstraction from THP occurs slightly later than that of THF (**6a**).

Table 3 reveals that the complexation of peroxy radical **3b** with THP (**1b)** affords a stabilization energy of 8.8–17.6 kJ mol^{-1} (ΔE_1). As observed in the reaction involving THF, the abstraction processes are predicted to be largely endothermic, in that the calculated energy barrier ($\Delta E_3^{\ddagger}$) for the reverse reaction (Scheme 4) is always larger than that ($\Delta E_2^{\ddagger}$) for the forward process. At the BHandHLYP/aug-cc-pVDZ//BHandHLYP/cc-pVDZ level of theory, the energy barriers for the reactions are calculated to be 104.1 and 36.0 kJ mol^{-1}, respectively, while values of 94.3 and 23.8 kJ mol^{-1} are calculated using the MPW1K/cc-pVDZ method. It should be noted that these barriers are not significantly different from those involving THF; energy barriers for the hydrogen abstraction reaction involving THP are calculated to be around 10 kJ·mol^{-1} higher than those involving THF.

Table 3 Energy barriers (in kJ·mol^{-1}) and imaginary frequencies (ν) for abstraction of α-hydrogen in THP

Method	ΔE_1	ΔE_1 +ZPE	$\Delta E_2^{\ddagger}$	$\Delta E_2^{\ddagger}$ +ZPE	$\Delta E_3^{\ddagger}$	$\Delta E_3^{\ddagger}$ +ZPE	ΔE_4	ΔE_4 +ZPE	ν (cm^{-1})
BHandHLYP/6-311G**	-14.6	-12.2	107.6	92.7	38.4	28.3	-6.8	-4.6	2253i
BHandHLYP/cc-pVDZ	-17.6	-14.9	106.9	91.5	35.2	24.5	-11.6	-8.9	2216i
BHandHLYP/aug-cc-pVDZ// BHandHLYP/cc-pVDZ	-8.8	--	104.1	--	36.0	--	0.3	--	--
MPW1K/cc-pVDZ	-14.0	-11.8	94.3	79.4	23.8	13.5	-8.3	-6.1	2007i

Table 4 Reaction energies (ΔE) and free energies (ΔG) (both in kJ·mol^{-1}) for autoxidation of THP

Method	$\Delta E_{coupling}$	$\Delta E_{coupling}$ +ZPE	$\Delta G_{coupling}$	$\Delta E_{H\text{-}abs}$	$\Delta E_{H\text{-}abs}$ +ZPE	$\Delta G_{H\text{-}abs}$	ΔE_{total}	ΔE_{total} +ZPE	ΔG_{total}
BHandHLYP/6-311G**	-140.1	-123.1	-78.9	61.3	56.8	55.8	-78.7	-66.3	-23.1
BHandHLYP/cc-pVDZ	-140.8	-124.1	-80.0	65.7	61.0	60.0	-75.1	-63.1	-20.0
BHandHLYP/aug-cc-pVDZ// BHandHLYP/cc-pVDZ	-138.2	-121.5	-77.1	59.0	55.0	54.4	-79.3	-66.5	-22.7
MPW1K/cc-pVDZ	-144.1	-127.5	-83.4	64.8	60.1	59.1	-79.3	-67.4	-24.2

The ΔE and ΔG values for the radical coupling, hydrogen abstraction, and overall reaction (Scheme 5) for the autoxidation of THP are listed in Table 4. The coupling reaction is predicted to be highly exothermic, the abstraction reaction is calculated to be endothermic, and the overall autoxidation reaction of THP is predicted to be exothermic. Similarly to the reaction involving THF, the free energies are smaller (by around 40 kJ·mol^{-1}) than the electronic energies with ZPE, while those for the hydrogen abstraction process are close to the electronic energies with ZPE; the free energies for the overall reaction are smaller than those of the electronic energies with ZPE by about 40 kJ·mol^{-1}. Not unexpectedly, this trend reflects that of the autoxidation process involving THF. Interestingly, ΔE and ΔG for the hydrogen abstraction involving THP are calculated to be around 15 kJ mol^{-1} more endothermic than those involving THF, whereas the overall reaction energies for the autoxidation of THP are predicted to be about 15 kJ mol^{-1} less exothermic than those for THF.

Calculations including solvation effects

Comparison of the autoxidation processes reveals that the activation energies are similar (~10 kJ·mol^{-1}) for both THF and THP. The negative ΔE and ΔG values for both compounds show that the transformations are exothermic/exergonic. These results indicate that only a slight difference in reactivity between the autoxidation of THF and that of THP would be predicted, which contradicts the experimental results. Thus, we carried out additional DFT calculations that included solvation effects. To consider solvent effects, the energy barriers (ΔE_1, $\Delta E_2^{\ddagger}$, $\Delta E_3^{\ddagger}$, and ΔE_4, Scheme 4) as well as the associated ΔE and ΔG values for the radical coupling and hydrogen abstraction (Scheme 5) for THF and THP were calculated at the BHandHLYP/aug-cc-pVDZ//BHandHLYP/cc-pVDZ level using the PCM method.[15] Similarly, the overall ΔE and ΔG values for the autoxidation process were obtained. The results are summarized in Table 5.

Table 5 BHandHLYP/aug-cc-pVDZ//BHandHLYP/cc-pVDZ calculated energy barriers (in kJ·mol^{-1}) of hydrogen abstraction, and reaction energies and free energies (ΔG) for autoxidation for THF and THP including solvent effects (PCM method, solvent = THF)

Compound	ΔE_1	$\Delta E_2^{\ddagger}$	$\Delta E_3^{\ddagger}$	ΔE_4	$\Delta E_{coupling}$	$\Delta G_{coupling}$	$\Delta E_{H\text{-}abs}$	$\Delta G_{H\text{-}abs}$	ΔE_{total}	ΔG_{total}
THF	-0.7	84.4	52.8	2.2	-146.7	-152.8	28.8	27.3	-117.9	-125.5
THP	-6.5	98.0	45.3	3.1	-138.8	-145.2	43.1	41.6	-95.8	-103.6

Table 5 shows that solvation effects do exert a significant influence on the energy barriers and reaction energies for the two ethers. For example, solvation effects decrease the energy barrier for the forward process ($\Delta E_2^{\ddagger}$) by 8–10 kJ·mol^{-1}, and increase the energy barrier for the reverse process ($\Delta E_3^{\ddagger}$) by 5–9 kJ·mol^{-1}. Solvation effects lower the endothermicity of the hydrogen abstraction process by about 15 kJ·mol^{-1}. On the other hand, the inclusion of solvation in calculations of the energy barriers ($\Delta E_2^{\ddagger}$) for the abstraction process in THF and THP predicts more significant differences between the two ethers. Namely, the energy barrier for the process with THP (including solvent effects) is calculated to be 15 kJ·mol^{-1} higher than that of THF. Nevertheless, this value would not be large enough to explain the difference in reactivity between THF and THP, which prompted us to investigate the first reaction step in the autoxidation reaction, the "radical coupling process" (Scheme 3), using DFT calculations.

Investigation of radical coupling process

We investigated the radical coupling process between complex **7a** and molecular oxygen (O_2) using the BHandHLYP/6-311G** level of theory. These calculations were carried out in doublet and quartet states. Namely, O_2 was treated as singlet and triplet states during the calculations. The calculated relative energy dependence of the complexes (**8a** and **8b**) involving THF and THP radicals (**2a** and **2b**) with O_2 at distance (*d*) between the ethers and the oxygen in the radical coupling process (Scheme 6)[16] are shown in Fig. 3 and 4, respectively.

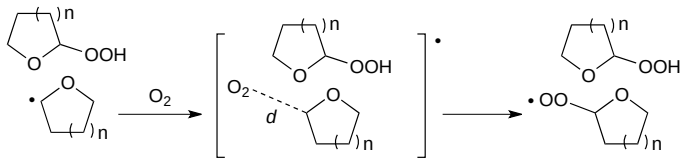

7a (n = 1) **7b** (n = 2) **8a** (n = 1) **8b** (n = 2) **9a** (n = 1) **9b** (n = 2)

Scheme 6 Reaction pathway for radical coupling process involved in the autoxidation of THF and THP.

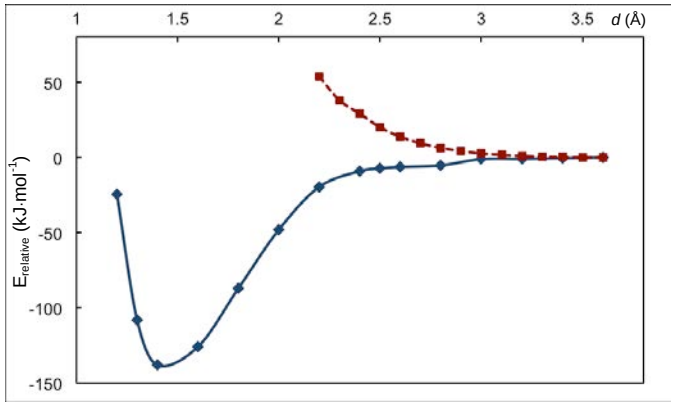

Fig. 3 BHandHLYP/6-311G**-calculated dependence of the energy of complex **8a** on distance (*d*) in the radical coupling reaction of complex **7a** involving THF radical with molecular oxygen. Solid line: calculation in the doublet state; dotted line: calculation in the quartet state.

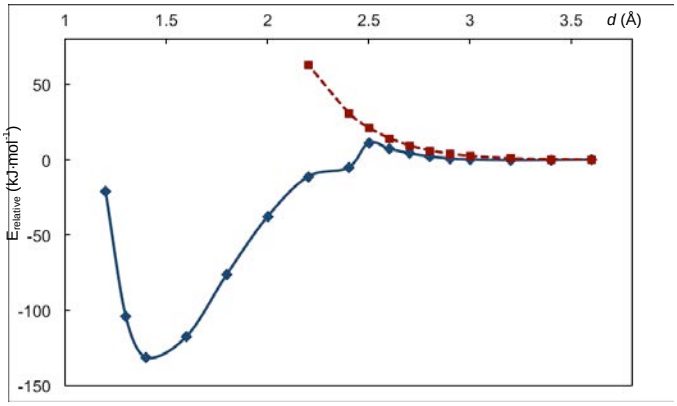

Fig. 4 BHandHLYP/6-311G** calculated dependence of the energy of complex **8b** on distance (*d*) in the radical coupling reaction of complex **7b** involving THP radical with molecular oxygen. Solid line: calculation in the doublet state; dotted line: calculation in the quartet state.

As shown in Fig. 3 and 4, the calculated energies involving triplet O_2 are close to those involving singlet O_2 when *d* between the THF or THP radical and O_2 is greater than 2.8 or 2.6 Å, respectively. However, when *d* is shorter than 2.8 (or 2.6) Å, the energies involving triplet O_2 increase dramatically, such that reactions with singlet O_2 become preferable. This indicates that reorientation of the spin (triplet to singlet) in O_2 may occur around *d* = 2.8 (or 2.6) Å to enable the reaction of O_2 with radical complexe **8a** (or **8b**). Interestingly, in the doublet state involving singlet O_2, the energy dependence on the distance is clearly illustrated, with the energy continuously decreasing as *d* is shortened in complex **8a** (THF), whereas an "energy barrier" exists as *d* is reduced in complex **8b** (THP). This energy barrier is calculated to be 11.2 kJ·mol^{-1}, which

would be large enough to obstruct the approach of O_2 to the THP radical moiety (**2b**). Indeed, the BHandHLYP/6-311G** optimization of **8a** involving the THF radical with d = 3 Å affords coupling product **9a**, whereas optimization of **8b** involving THP at the same distance provides complex **7b**, and no coupling product **9b** is obtained.

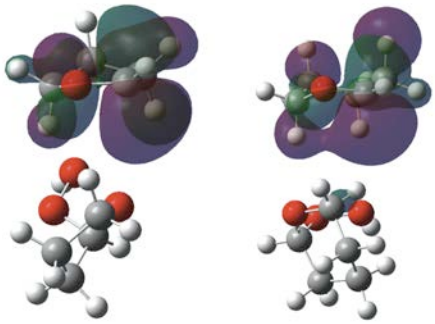

Fig. 5 The Kohn–Sham SOMOs (surface of absolute isovalue = 0.02) in complexes **7a** (left) and **7b** (right) generated at the BHandHLYP/6-311G** level.

The Kohn−Sham singly occupied molecular orbitals (SOMOs) (surface of absolute isovalue is 0.02) in complexes **7a** and **7b** generated at the BHandHLYP/6-311G** level are displayed in Fig. 5. Inspection of the figure reveals that, whereas the SOMO of complex **7a** involving the THF radical extends downward, the SOMO of complex **7b** involving the THP radical is significantly smaller; the reaction site (radical) would be blocked by the hydrogen atoms of the THP ring when molecular oxygen approaches the complex.

Conclusions

Ab initio and DFT calculations predict that the energy barrier for hydrogen abstraction from THP would be slightly higher (by around 10 kJ·mol^{-1}) than that from THF. The calculated reaction energies indicate that hydrogen abstraction from THP would be more endothermic by about 15 kJ·mol^{-1} than that of THF. The inclusion of solvation into the calculations has little influence on the energy barriers and reaction energies for any step of the autoxidation process. For example, the calculated energy barrier for hydrogen abstraction from THP (with solvent) is 14 kJ·mol^{-1} higher than that from THF, and the reaction energy of the THP autoxidation reaction (with solvent) is calculated to be 22 kJ·mol^{-1} more exothermic than that involving THF; the difference with and without solvent effects is calculated to be around 5 kJ·mol^{-1}. The process of molecular oxygen capture by the generated THF (or THP) radical was then investigated using the BHandHLYP/6-311G** level of theory, and a significant energy barrier (11.2 kJ·mol^{-1}) was predicted to exist for the process involving THP, whereas no equivalent barrier was found for the THF reaction. The Kohn-Sham SOMO in radical complex **7b** from THP is smaller than that of THF; the orbital is predicted to be surrounded by the hydrogen atoms of the THP ring, which prevent molecular oxygen from approaching the complex. These factors—the larger energy barriers for the hydrogen abstraction process, the existence of an "energy barrier" in the process of capturing molecular oxygen, and the smaller and shielded SOMO—all work together to make the autoxidation of THP much slower than that of THF.

Acknowledgements

This work was partially supported by a Grant-in-Aid for Scientific Research from the JSPS. We thank Dr. Sara H. Kyne for useful suggestions on the manuscript.

Notes and references

Department of Chemistry, Graduate School of Science, Osaka Prefecture University Sakai, Osaka 599-8531, Japan. E-mail: matsu@c.s.osakafu-u.ac.jp

Electronic Supplementary Information (ESI) available: Fig. S1–S6, Table S1, a full list of reference 10 and Gaussian Archive entries for the optimized complexes and transition states in this study and higher-level calculated single-point energies. See DOI: 10.1039/b000000x/

1 For example, see: M. B. Smith, *March's Advanced Organic Chemistry*, 2013, Wiley, New Jersey, 7th edition, p.713.

2 For some recent work on oxidation of ethers, see: (a) S. Di Tommaso, P. Rotureau, B. Sirjean, R. Fournet, W. Benaissa, P. Gruez and C. Adamo, *Proc. Safety Prog.*, 2014, **33**, 64; (b) S. Di Tommaso, P. Rotureau, O. Crescenzi and C. Adamo, *Phys. Chem. Chem. Phys.*, 2011, **13**, 14636; (c) H. Hoshino, K. Sakakibara and K. Watanabe, *Chem. Lett.*, 2008, **37**, 774.

3 (a) A. Rieche and R. Meister, *Angew. Chem.*, 1936, **49**, 101; (b) A. G. Davies, *J. Roy. Inst. Chem.*, 1956, **80**, 386; (c) G. T. Morgan and R. H. Pickard, *Chem. Ind.*, 1936, 421.

4 J. A. Howard and K. U. Ingold, *Can. J. Chem.*, 1970, **48**, 873.

5 H. Yasuda, Y. Uenoyama, O. Nobuta, S. Kobayashi and I. Ryu, *Tetrahedron Lett.*, 2008, **49**, 367.

6 For some of our recent work on computational investigations of radical reactions, see: (a) T. Kawamoto, H. Matsubara and I. Ryu, *Chem. Lett.*, 2014, **43**, 1140; (b) S. H. Kyne, C. H. Schiesser and H. Matsubara, *Org. Biomol. Chem.*, 2011, **9**, 3217; (c) S. H. Kyne, C. H. Schiesser and H. Matsubara, *J. Org. Chem.*, 2008, **73**, 427; (d) S. H. Kyne, C. H. Schiesser and H. Matsubara, *Org. Biomol. Chem.*, 2007, **5**, 3938; (e) H. Matsubara, I. Ryu and C. H. Schiesser, *Org. Biomol. Chem.*, 2007, **5**, 3320; (f) C. H. Schiesser, U. Wille, H. Matsubara and I. Ryu, *Acc. Chem. Res.*, 2007, **40**, 303.

7 For some work involving peroxy radicals, see: (a) K. U. Ingold, *Acc. Chem. Res.*, 1969, **2**, 1; (b) Y. Yamamoto, K. Yamada, K. Tomioka, *Tetrahedron Lett.*, 2004, **45**, 795; (c) G. A. DiLabio, K. U. Ingold, J. C. Walton, *J. Org. Chem.*, 2007, **72**, 8095.

8 The energies for other hydrogen transfer mechanisms including single electron transfer (SET) and asynchronous proton transfer were also calculated. The reaction energies (ΔE) in THF solvent for SET and proton transfer are *ca.* 365 and −330 kJ·mol^{-1} respectively, indicating that these processes would not be preferable. See Table S1 in the ESI.

9 In order to examine whether tunnelling effects play a significant role in the hydrogen abstraction process, tunnelling transmission probability using an unsymmetrical Eckart barrier model (H. S. Johnston, J. Heicklen, *J. Phys. Chem.*, 1962, **66**, 532) were calculated. The tunnelling transmission probability for hydrogen abstraction from THF using the BHandHLYP/6-311G** data was calculated to be 3.6×10^{-5}, indicating that the tunnelling effect is not important for this process.

10 M. J. Frisch, *et al*., *GAUSSIAN 03 (Revision E.01)*, Gaussian Inc., Wallingford, CT, 2004; M. J. Frisch *et al.*, *GAUSSIAN 09 (Revision C.01)*, Gaussian Inc., Wallingford, CT, 2010.
11 B. J. Lynch, P. L. Fast, M. Harris and D. G. Truhlar, *J. Phys. Chem. A*, 2000, **104**, 4811.
12 Y. Zhao, N. González-García and D. G. Truhlar, *J. Phys. Chem. A*, 2005, **109**, 2012.
13 Y. Zhao, N. E. Schultz, and D. G. Truhlar, *J. Chem. Phys.*, 2005, **123**, 161103.
14 D. J. Henry, M. B. Sullivan and L. Radom, *J. Chem. Phys.*, 2003, **118**, 4849.
15 J. Tomasi, B. Mennucci, and R. Cammi, *Chem. Rev.*, 2005, **105**, 2999.
16 The radical coupling process for the initial step of the first cycle, *i.e*., the reaction between the THF (or THP) radical with molecular oxygen (singlet or triplet state) was also examined at the BHandHLYP/6-311G** level, and is summarized in Fig. S5 and S6 in the ESI. The reaction profiles are similar to those observed after the second cycle.

